

# Effect of CO<sub>2</sub> on the properties and sinking velocity of aggregates of the coccolithophore *Emiliana huxleyi*

A. Biermann<sup>1,\*</sup> and A. Engel<sup>1</sup>

<sup>1</sup>Alfred Wegener Institute for Polar and Marine Research, Am Handelshafen 12, 27570 Bremerhaven, Germany

\* present address: IFM-GEOMAR, Leibniz Institute of Marine Sciences, Düsternbrooker Weg 20, 24105 Kiel, Germany

Received: 8 September 2009 – Published in Biogeosciences Discuss.: 13 October 2009

Revised: 16 February 2010 – Accepted: 23 February 2010 – Published: 17 March 2010

**Abstract.** Coccolithophores play an important role in organic matter export due to their production of the mineral calcite that can act as ballast. Recent studies indicated that calcification in coccolithophores may be affected by changes in seawater carbonate chemistry. We investigated the influence of CO<sub>2</sub> on the aggregation and sinking behaviour of the coccolithophore *Emiliana huxleyi* (PML B92/11) during a laboratory experiment. The coccolithophores were grown under low (~180 μatm), medium (~380 μatm), and high (~750 μatm) CO<sub>2</sub> conditions. Aggregation of the cells was promoted using roller tables. Size and settling velocity of aggregates were determined during the incubation using video image analysis. Our results indicate that aggregate properties are sensitive to changes in the degree of ballasting, as evoked by ocean acidification. Average sinking velocity was highest for low CO<sub>2</sub> aggregates (~1292 m d<sup>-1</sup>) that also had the highest particulate inorganic to particulate organic carbon (PIC/POC) ratio. Lowest PIC/POC ratios and lowest sinking velocity (~366 m d<sup>-1</sup>) at comparable sizes were observed for aggregates of the high CO<sub>2</sub> treatment. Aggregates of the high CO<sub>2</sub> treatment showed a 4-fold lower excess density (~4.2 × 10<sup>-4</sup> g cm<sup>-3</sup>) when compared to aggregates from the medium and low CO<sub>2</sub> treatments (~1.7 g × 10<sup>-3</sup> cm<sup>-3</sup>). We also observed that more aggregates formed in the high CO<sub>2</sub> treatment, and that those aggregates contained more bacteria than aggregates in the medium and low CO<sub>2</sub> treatment. If applicable to the future ocean, our findings suggest that a CO<sub>2</sub> induced reduction of the calcite content of aggregates could weaken the deep export of organic matter in the ocean, particularly in areas dominated by coccolithophores.

## 1 Introduction

In times of rising atmospheric CO<sub>2</sub>, the marine carbon cycle receives special attention. The ocean is the largest sink for atmospheric CO<sub>2</sub> (Sabine et al., 2004) due to the physical uptake of CO<sub>2</sub>, the chemical conversion of CO<sub>2</sub> into bicarbonate and carbonate, and the sequestration of carbon into deeper layers of the ocean via the vertical export of organic matter, i.e. the biological pump. A small fraction of exported carbon is deposited in the worlds' oceans sediments where it is partly conserved on a time scale of years to millennia.

The major fraction of organic matter is transported to the deep ocean by aggregates, in form of marine snow or fecal pellets (Honjo, 1982; Fowler and Knauer, 1986). Biogenic minerals or lithogenic particles of eolian or riverine origin can act as ballast to organic matter because of their higher density (Ittekkot and Haake, 1990). Recent findings suggest that the flux of organic matter at depth ~1800 m is directly related to the fluxes of ballast minerals (Armstrong et al., 2002; Francois et al., 2002; Klaas and Archer, 2002). Thereby, the mineral phase may protect organic matter from degradation, or the organic matter may serve as glue that binds mineral and organic particles together, or mineral-organic aggregates may disintegrate if the organic matter content becomes too low (Armstrong et al., 2002). A comparison of sediment trap data below 1000 m from 52 locations around the world confirmed that most of the organic carbon that is transferred to the deep sea is carried by calcium carbonate (Klaas and Archer, 2002).

Coccolithophores are unicellular algae, readily abundant in temperate and sub-polar regions of the oceans, and well known to develop large blooms with densities of up to several 10<sup>5</sup> cells ml<sup>-1</sup> seawater (Holligan et al., 1983; Robertson et al., 1991; van der Wal et al., 1995; Kleypas, 2006; Raitos et al., 2006). Coccolithophores also provide the majority of



Correspondence to: A. Biermann  
(abiermann@ifm-geomar.de)

**Table 1.** Chemical and biological characteristics of the cell suspension (per volume suspension) before the roller table experiment was started (T14). For  $p\text{CO}_2$  the mean partial pressure during the inoculation from T1 to T14 is given.

Parameter	Unit	LCT	MCT	HCT
TPV	mm <sup>3</sup> L <sup>-1</sup>	82.8	112	91.0
TPC	mg L <sup>-1</sup>	29.9±1.38	47.3±0.465	40.7±2.02
POC	mg L <sup>-1</sup>	19.0±1.42	33.8±0.978	31.9±1.53
PIC	mg L <sup>-1</sup>	10.9±2.59	13.5±1.04	9.42±4.00
PN	mg L <sup>-1</sup>	2.13±0.08	1.90±0.082	1.86±0.114
DW	mg L <sup>-1</sup>	778±64.5	908±48.5	750±110
Bacteria	L <sup>-1</sup>	7.27×10 <sup>8</sup>	3.20×10 <sup>9</sup>	1.95×10 <sup>9</sup>
PIC/POC	mol/mol	0.579±0.177	0.399±0.041	0.298±0.140
TPC/PN	mol/mol	17.5±0.223	31.2±1.03	27.5±0.334
POC/PN	mol/mol	11.2±1.23	22.3±1.14	21.3±2.65
$p\text{CO}_2$ aeration (T1–T14)	µatm	207±87 (n=31)	402±8 (n=7)	728±200 (n=36)
CO <sub>2</sub> calculated	µmol L <sup>-1</sup>	0.133	3.68	24.2
Ω <sub>calcite</sub>	–	6.3	2.3	1.3

biogenic calcite in the ocean by precipitating a sphere of calcium carbonate (calcite) platelets, the coccoliths (Winter et al., 1994; Paasche, 2002; Kleypas, 2006). In experimental studies with the coccolithophore *E. huxleyi*, increased CO<sub>2</sub> concentrations led to lower rates of calcite precipitation when compared to organic matter production (Riebesell et al., 2000; Zondervan et al., 2001, 2002). However, other studies report of either an opposite effect of elevated CO<sub>2</sub> concentrations on coccolithophores (Iglesias-Rodriguez et al., 2008) or suggest a strain-specific response of *E. huxleyi* under increased CO<sub>2</sub> levels (Langer et al., 2009).

A study, comparing aggregates that were formed by calcifying cells of *E. huxleyi* with those formed by cells that lack a coccosphere, revealed that calcite has a strong effect on aggregate properties (Engel et al., 2009b). Calcareous aggregates had higher excess density and settling velocity. It was also demonstrated that aggregates without coccoliths were more prone to decomposition (Engel et al., 2009a).

In general, the composition of an aggregate determines its properties, such as size, porosity, excess density, or drag coefficient (Alldredge and Gotschalk, 1988; Engel and Schartau, 1999). The relationship between aggregate composition and these properties, however, is complex, and effects of compositional changes on the resulting physical behaviour of an aggregate, e.g. its sinking velocity or break-up, can hardly be predicted.

So far, it is not known how sensitive aggregate properties and settling velocity respond to changes in aggregate composition, e.g. the degree of ballasting, that are evoked by ocean acidification.

Here, we investigate how different CO<sub>2</sub> concentrations during an *E. huxleyi* bloom may affect the formation, properties and sinking velocity of aggregates, and discuss potential implications for organic matter export in the future ocean.

## 2 Methods

### 2.1 Experimental setup

The calcifying strain *Emiliania huxleyi* (PML B92/11) was grown in 20-L bottles at three different CO<sub>2</sub> conditions for 13 days and ~13 generations. Adjustment of the  $p\text{CO}_2$  was achieved by an aeration system: in order to simulate a low CO<sub>2</sub> treatment (LCT) with concentrations typical for the last glacial maximum (~180 µatm), pure CO<sub>2</sub> was mixed with CO<sub>2</sub>-free air. The medium CO<sub>2</sub> treatment (MCT) of ~380 µatm CO<sub>2</sub> represents today's atmospheric CO<sub>2</sub> condition, and was conducted with ambient air. The high CO<sub>2</sub> treatment (HCT) of ~750 µatm, simulated the year 2100 as predicted by the IS92a scenario of the Intergovernmental Panel on Climate Change (IPCC, 2001). The concentration for HCT was achieved by mixing pure CO<sub>2</sub> with CO<sub>2</sub>-free air. The flow rate of the two gases was adjusted manually by means of hose clips. For control of the final CO<sub>2</sub> concentration, a LICOR Li-6252 gas analyzer was used. By bubbling the gas from the bottom of the bottles, the cultures were kept well mixed. The cells were grown in 0.2 µm filtered North Sea water with a salinity of 32.3 (Cond 330i, WTW), and at a temperature of 17±0.2 °C. The water was enriched with nutrients to yield 155 µmol L<sup>-1</sup> NaNO<sub>3</sub> and 11 µmol L<sup>-1</sup> Na<sub>2</sub>HPO<sub>4</sub> initially. In addition, trace nutrients were added according to the f/2 recipe of Guillard and Ryther (1962). The day to night cycle was adjusted to 16:8 h with a light intensity during day hours of 218±10 µmol photons m<sup>-2</sup> s<sup>-1</sup>. Prior to the experiment, all tubes and bottles were either autoclaved or washed with 10% HCl, and rinsed thoroughly with MilliQ water thereafter.

Because aggregate formation has most often been observed towards the end of phytoplankton blooms, the

aggregation experiment was started after 7 days of the stationary growth (T14; Table 1). At this time, the cultures were transferred into a total of nine transparent, cylindrical tanks.

For each treatment one 10-L tank and two 4.5-L tanks were filled and immediately put onto roller tables. The roller table experiments started at a cell abundance of  $2.6 \times 10^6$  cells ml<sup>-1</sup> for LCT,  $2.2 \times 10^6$  cells ml<sup>-1</sup> for the MCT and  $2.5 \times 10^6$  cells ml<sup>-1</sup> for the HCT. Although natural blooms achieve lower cell densities of up to  $3.5 \times 10^5$  cells ml<sup>-1</sup> (Robertson et al. 1991), we chose higher abundances to assure that enough cell material was present for aggregate formation and subsequent chemical analysis. The rotation speed was set to  $2.35 \pm 0.05$  rpm. During the experiment, the rotation speed of tanks was repeatedly increased in order to prevent the aggregates from colliding with the tank walls (Engel et al., 2009b).

The pH in the tanks was determined during the roller table experiment in one of the 4.5-L tanks of each treatment at T<sub>18</sub>, yielding values of 8.9, 7.9 and 7.6 for the LCT, MCT and HCT, respectively.

The 10-L tanks were used for recording aggregates with a video camera. Video pictures were analyzed using image analysis and sinking velocity and other aggregate properties were determined after Engel and Schartau (1999). Aggregates were filmed each day twice for 10 min with a digital camera (Sony digital 8 DCR-TRV460) equipped with an 80-mm macro lens. The distance between the 4 cm × 5 cm observation area (x/y coordination grid) and the lens was 5 cm. The observation area was chosen on the right side in the middle of the horizontal axis, since the tank was rotating anti-clockwise and aggregates accumulated in this area (Tooby et al., 1977). Additionally, a mm-scale was put onto the tank at the observation area for determining the aggregates sizes. The videos were recorded to a PC with the software Pinnacle Studio Plus 700-PCI, and single pictures were analysed using ImageJ 1.38 (Wayne Rasband, National Institutes of Health, Bethesda, Maryland, USA). Aggregates were marked and the following parameters determined: their position ( $x, y$ ), area, length of the longest axis (major), length of the shortest axis (minor) and x-feret diameter ( $d_f$ ), which is the largest size of an aggregate perpendicular to the direction of the fall. The number of analyzed aggregates was  $n=71$  for the LCT, and  $n=63$  and  $n=65$  for the MCT and HCT, respectively.

For the dimensionless drag coefficient ( $C_d$ ) we assumed a value of  $95 (Re)^{-1.85}$  after Alldredge and Gotschalk (1988) and  $Re=dU/\nu$ , where  $d$  is the particle diameter,  $U$  is the sinking velocity of the particle, and  $\nu$  the kinematic viscosity of the fluid. The kinematic viscosity of the fluid is the quotient of dynamic viscosity ( $\zeta$ ) and the density of the fluid ( $\rho_f$ ). The dynamic viscosity ( $\zeta$ ) was  $0.0118 \text{ cm}^2 \text{ s}^{-1}$ , interpolated according to Dietrich et al. (1975) for a temperature of 17 °C and salinity of 32.3. The calculated kinematic viscosity was  $0.01153 \text{ cm}^2 \text{ s}^{-1}$ .

The porosity ( $P$ ) of an aggregate was calculated according to (Engel and Schartau, 1999):

$$P = 1 - (\Delta\rho/p_p) \quad (1)$$

Here,  $\Delta\rho$  is the excess density ( $\text{g cm}^{-3}$ ) and  $p_p$  is the density of the particle, assumed to be  $1.19 \text{ g cm}^{-3}$  for fully calcified cells of the LCT aggregates (Fig. 5a), according to Paasche (2002). For the less calcified and naked cells of MCT and HCT (Fig. 5b), we calculated the porosity assuming a minimum cell density of  $1.095 \text{ g cm}^{-3}$ , as determined for non-calcified cells by Engel et al. (2009b). The value of  $\Delta\rho$  of an aggregate was derived from settling velocity according to Engel and Schartau (1999).

The mass of the single aggregate was calculated from  $\Delta\rho$  multiplied with its volume ( $V_{ag}$ ) as derived from the video picture analysis:

$$\text{Mass} = \Delta\rho \times V_{ag}. \quad (2)$$

Note, for a better distinction we use the term “mass” for data that was derived from the video picture analysis, whereas the term “dry weight (DW)” of an aggregate is used for data obtained from weight measurements.

## 2.2 Sampling

On four days samples were taken for the analyses of bacteria, nutrients, scanning electron microscopy (SEM), total alkalinity (TA), total particulate carbon (TPC), particulate organic and inorganic carbon (POC and PIC), total particulate nitrogen (PN), dry weight (DW), cell counts and total particle volume (TPV), and pH.

On the last day of the experiment (T21), all tanks were removed carefully from the rolling tables and turned to one side. About 15 min after, the aggregates had settled to the bottom and were isolated from the surrounding cell suspension using a 10 ml serological pipette. From each tank, all visible aggregates ( $> 1$  mm) were collected, pooled and the total amount of aggregate slurry was determined. Afterwards, the slurry was diluted with one litre of NaCl solution, adjusted to sample salinity. Samples were also taken from the surrounding cell suspension (SUSP) containing no visible aggregates. To determine the total amount of particulate matter within the aggregate fraction (AGG), the amount of particulate constituents determined for the slurry (SL) was corrected for particulate material by-harvested from SUSP according to:

$$(x)_{AGG} = (V_{SL} \times cx_{SL}) - (V_{SL} \times cx_{SUSP}) \quad (3)$$

where  $V_{SL}$  is the volume of the slurry,  $cx_{SL}$  is the concentration of a parameter  $x$  of the slurry,  $cx_{SUSP}$  is the concentration of a component  $x$  of the background suspension (Engel et al., 2002).

### 2.3 Chemical analyses, cell counts, total particle volume (TPV) and SEM

For the determination of nutrients, 50 ml of sample were 0.2 µm filtered (Minisart) and stored at -20 °C until photometrical processing using an auto analyser (Evolution 3, Alliance Instruments). Determinations were performed in duplicate after the method of Grashoff et al. (1999). The detection limit was 0.3 µmol L<sup>-1</sup> for NO<sub>3</sub><sup>-</sup> and 0.1 µmol L<sup>-1</sup> for PO<sub>4</sub><sup>3-</sup>. Abundance and volume of cells in the size range 2.751–5.789 µm equivalent spherical diameter (ESD) were determined with a coulter counter (Multisizer 3, Beckman). A volume of 0.2–4 ml of samples diluted with 16–20 ml of 0.2 µm filtered seawater was measured in triplicate. Sample dilution was necessary in order to keep the coincidence of particles at the 100 µm aperture <5%. The total particle volume (TPV) was determined as the sum of volumes of individual particles. The pH and temperature were determined with a WTW pH meter (model 340 i) at day T0, T6, T14 and T21. Alkalinity was determined at these days from 200 ml sample filtered through combusted (8 h at 500 °C) GF/F filters (Whatman). The samples were stored in the dark at 0 °C until analysis by potentiometric titration (Brewer et al., 1986), using a Metrohm 665 dosimeter and a 713 pH-meter. Total alkalinity (TA) was calculated from Gran plots (Gran, 1952). The calcite saturation state ( $\Omega$ ) was calculated with the help of pH (NBS scale) and TA, using the software CO2SYS (Lewis and Wallace, 1998). In CO2SYS, we used the carbonic acid dissociation constant from Mehrbach et al. (1973), refitted by Dickson and Millero (1987). The dissociation constants for the reaction  $\text{HSO}_4^- = \text{H}^+ + \text{SO}_4^{2-}$  were taken from Dickson (1990a), and the solubility product for calcite calculated after Mucci (1975). Dry weight (DW) of particulate matter was determined from 10–100 ml taken at T0, T6, T14, and T21 and filtered gently (<200 mbar) onto combusted (8 h, 500 °C) and pre-weighed GF/F filters (Whatman). The filters were oven dried for 24 h at 60 °C and reweighed. For total particulate carbon (TPC), particulate organic carbon (POC), and total particulate nitrogen (PN), 10–100 ml were filtered onto combusted (8 h, 500 °C) GF/F filters (Whatman) and measured on an elemental analyzer (model Euro EA). Before elemental analysis, filters were dried for 24 h at 60 °C. For POC, one set of filters was acidified with 5 to 8 drops of 0.1 N HCl in order to remove inorganic carbon. Particulate inorganic carbon (PIC) was then calculated by subtracting POC from TPC. Filters for dry weight, TPC, PN, POC, and PIC were stored at -20 °C until analysis. At T0 and T6 only single filters were prepared for each treatment, whereas triplicates for SUSP and AGG were obtained at T14 and T21.

For bacterial abundance, 5 ml of both SUSP and aggregate slurry were collected in duplicate at T14 and in triplicate at T21 (Table 1), preserved with Glutaraldehyde (GDA) to an end concentration of 0.023%, and frozen at -20 °C until measurement. Bacterial abundance was determined with

a Becton Dickinson FacsCalibur flow cytometer and using CellQuest 3.3 (Becton Dickinson) and WinMD 2.8 (J. Trotter, The Scripps Institute, La Jolla, CA). The flow cytometer was equipped with an air cooled argon laser (15 mW, Ex. 488 nm). Fluorescence (FL1) was detected with a standard filter set-up (Em. 530±15 nm) and analyses performed at the lowest flow rate (approx. 14 µl min<sup>-1</sup>). Event range was between 200 and 800 s<sup>-1</sup>. Prior to measurement, 20 µl of sample was diluted with deionised water to a concentration of 10%. Bacteria then were stained with 5 µl of the fluorescence dye SybrGreen I (Invitrogen) diluted in Dimethyl Sulfoxide (DMSO) to an end concentration of 2.5%. 5 µl fluorescent beads (Polyscience) were used for the internal volume normalization and calibrated against TruCount beads (Becton Dickinson) for absolute volume concentration calculation. After the visual inspection of the dot plots of FL 1 and side scatter (SSC) a manual gating was performed (Gasol and Giorgio, 2000).

An overview of the results of chemical analyses of suspensions before transfer to the roller tanks (T14) is given in Table 1.

For scanning electron microscopy (SEM), 5 to 15 ml of sample were filtered (<200 mbar) onto 0.2 µm polycarbonate filters (Sartorius), dried, and sputtered with gold-palladium. Analysis was made with a Qanta 200 F (Fei) electron microscope. For each CO<sub>2</sub> treatment and sampling day 5 to 12 pictures were made and analysed qualitatively within a magnification range of 1000× to 40 000×.

### 2.4 Statistics

Nonlinear curve fits were performed with SigmaPlot 10.0 (SysStat). The treatments were compared by analysis of variance (ANOVA), significant differences calculated with Tukey's HSD test, and homogeneity of variances checked with Levene's test (Statistica 8.0, StatSoft). Additionally, Kruskal-Wallis tests were performed for non-normal distributed data. Statistical significance was accepted for  $p < 0.05$ .

## 3 Results

### 3.1 Aggregate properties derived from video picture analysis

#### 3.1.1 Aggregate shape, size and sinking velocity

Visible aggregates appeared within 12 h in all roller tanks. The shape of aggregates clearly differed between the CO<sub>2</sub> treatments (pictures not shown). While aggregates that formed in the LCT were compact and spherical, aggregates of the HCT treatment seemed to be more fragile, fluffy and elongated. Aggregates of the MCT took in an intermediate position, being not as compact as the LCT aggregates but also spherical.

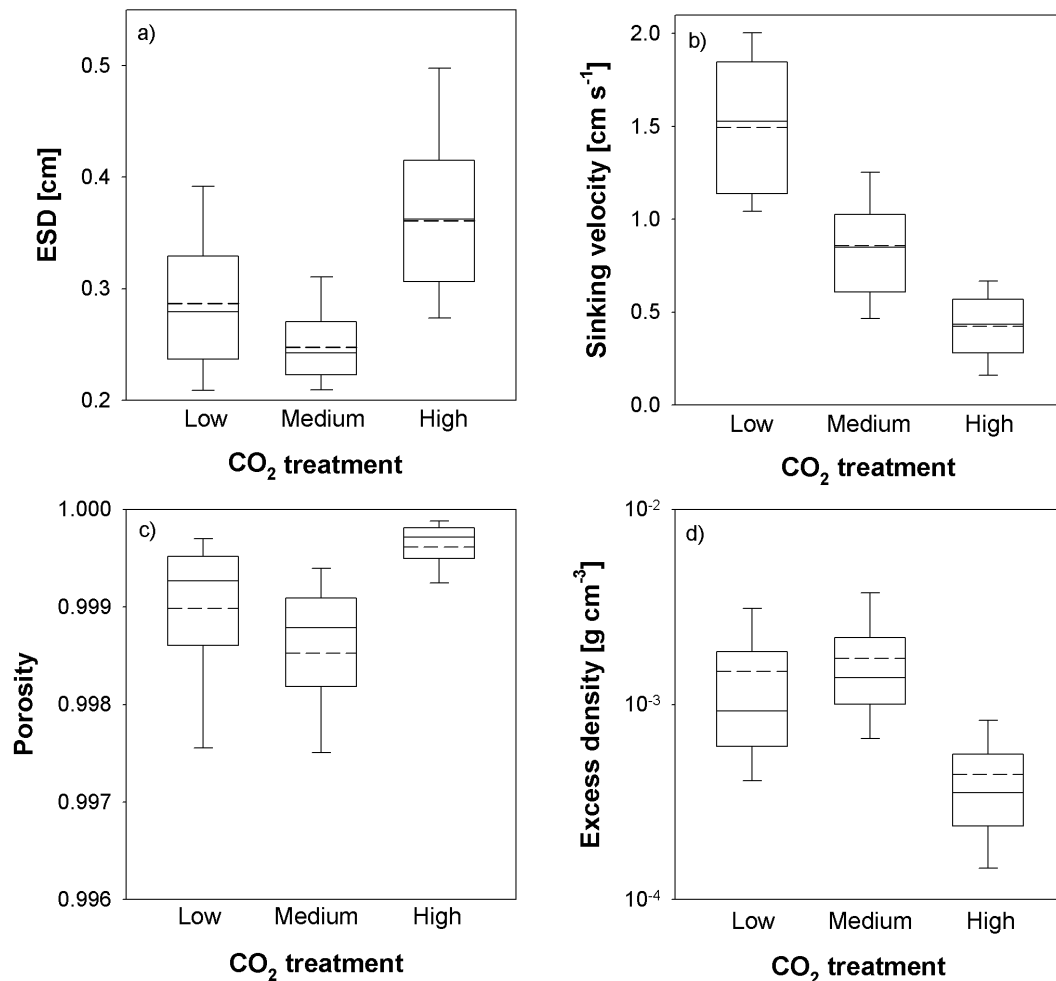


**Fig. 1.** (a) equivalent spherical diameter (ESD), (b) sinking velocity, (c) porosity and (d) excess density of aggregates in the three CO<sub>2</sub> treatments during the roller table experiment. Pooled data of four days (T14–T18) during the incubation (LCT:  $n=71$ , MCT:  $n=62$ , HCT:  $n=65$ ). Median = solid line, mean = dashed line. Length of the box expresses the spread of the data set (25–75%), error bars (10–90%).

Figure 1a shows the size of aggregates for the different treatments, displayed as the equivalent spherical diameter (ESD) of an aggregate. The largest aggregates were observed in the HCT, with an average size of  $0.367\text{ cm} \pm 0.090$  and a maximum size of  $0.669\text{ cm}$ . Aggregates of the LCT were significantly smaller than in the HCT ( $p < 0.001$ ), reaching on average  $0.268 \pm 0.085\text{ cm}$  and a maximum size of  $0.565\text{ cm}$ . The smallest aggregates were those of the MCT with on average  $0.230 \pm 0.061\text{ cm}$  (MCT vs. LCT:  $p < 0.05$ , MCT vs. HCT  $p < 0.001$ ) and a maximum size of  $0.346\text{ cm}$ . In addition, the variability of aggregate sizes was smallest for MCT.

The sinking velocity of aggregates differed significantly ( $p < 0.001$ ) between the CO<sub>2</sub> treatments (Fig. 1b). Although the aggregates of the HCT were largest, their sinking velocity was the lowest of all CO<sub>2</sub> treatments. Sinking velocity of HCT aggregates was on average  $0.4\text{ cm s}^{-1}$  or  $366\text{ m d}^{-1}$ . MCT aggregates were sinking with an average rate of  $0.9\text{ cm s}^{-1}$  or  $740\text{ m d}^{-1}$ . Sinking velocities of

LCT aggregates were the fastest with on average  $1.5\text{ cm s}^{-1}$ ,  $1292\text{ m d}^{-1}$ , respectively.

A non-linear relationship between aggregate size ( $x$ , cm) and sinking velocity ( $y$ ,  $\text{cm s}^{-1}$ ) was determined for aggregates of the LCT, yielding  $y = 3.75x^{0.7}$  ( $r^2 = 0.58$ ). For MCT and HCT aggregates, size and sinking velocity were not correlated (Fig. 2).

### 3.1.2 Porosity, excess density, and mass of aggregates

The porosity of HCT aggregates was on average  $99.96 \pm 0.03\%$ , and significantly higher ( $p < 0.001$ ) than porosities of MCT and LCT aggregates, which were more similar with  $99.85 \pm 0.09\%$  and  $99.86 \pm 0.2\%$ , respectively (Fig. 1c).

The excess densities ( $\Delta\rho$ ) of HCT aggregates were significantly different from those of MCT and LCT aggregates ( $p < 0.001$ ) (Fig. 1d). The  $\Delta\rho$  for HCT was on average

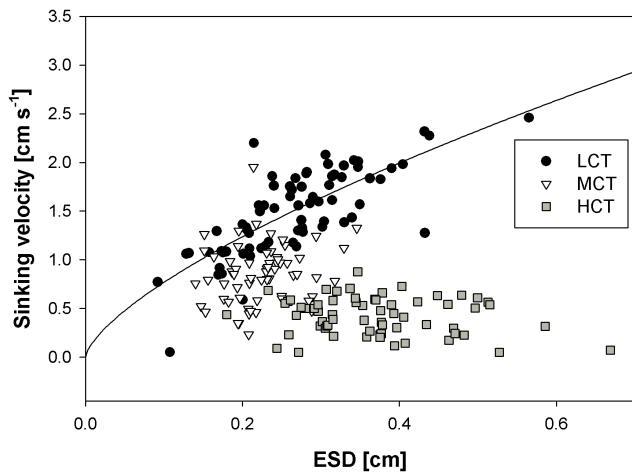


**Fig. 2.** Sinking velocity ( $\text{cm s}^{-1}$ ) in relation to the equivalent spherical diameter (ESD, cm) of the aggregates in the three CO<sub>2</sub> treatments during the roller table experiment. The curve fit to the LCT (filled dots) is  $y=3.75x^{0.7}$  ( $r^2=0.58$ ) (for  $n$  see Fig. 1).

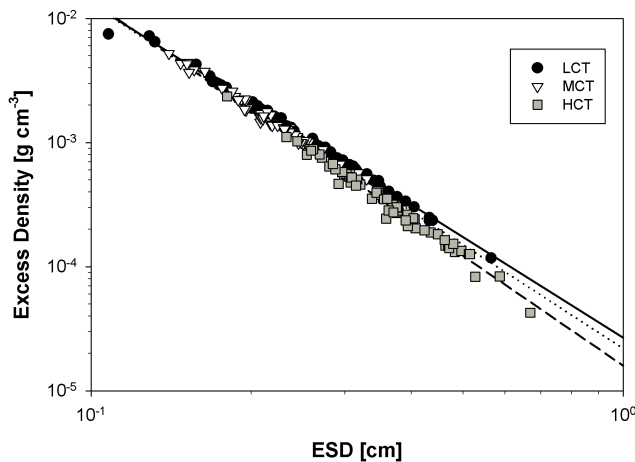


**Fig. 3.** Excess density ( $\text{g cm}^{-3}$ ) in relation to the equivalent spherical diameter (ESD, cm) of the aggregates in the three CO<sub>2</sub> treatments during the roller table experiment. (For  $n$  see Fig. 1). The excess density of aggregates was related to the ESD with the power decay function for LCT:  $y=3 \times 10^{-5}x^{-2.69}$  ( $r^2=0.99$ ) (solid line), for MCT:  $y=2 \times 10^{-5}x^{-2.78}$  ( $r^2=0.99$ ) (dotted line) and for HCT:  $y=2 \times 10^{-5}x^{-2.94}$  ( $r^2=0.99$ ) (dashed line).

$4.2 \times 10^{-4} \pm 3.4 \times 10^{-4} \text{ g cm}^{-3}$  and clearly smaller than the  $\Delta\rho$  of MCT and LCT aggregates. Aggregates of the MCT had an average  $\Delta\rho$  of  $1.7 \times 10^{-3} \pm 1.1 \times 10^{-3} \text{ g cm}^{-3}$ , not different from the average  $\Delta\rho$  of LCT aggregates yielding  $1.7 \times 10^{-3} \pm 2.4 \times 10^{-3} \text{ g cm}^{-3}$ . For all aggregates, a general decrease in  $\Delta\rho$  with size was observed (Fig. 3). At comparable size, the  $\Delta\rho$  of MCT aggregates took in an intermediate position between LCT and HCT aggregates.

The mass ( $\mu\text{g}$ ) of LCT aggregates was related to the equivalent spherical diameter (ESD, cm) in the power function

**Table 2.** Slurry volumes of each tank that were isolated after the roller table experiment.

Tank vol.	Slurry volume [ml]		
	LCT	MCT	HCT
10L	77.1	69.8	117.9
4.5 L a	21.4	86.7	97.5
4.5 L b	21.6	14.9	96.0
Total	120.1	171.4	311.4

mass =  $13.6 \text{ ESD}^{0.28}$  ( $r^2=0.79$ ) (Fig. 4a). The relationship between mass and size was less pronounced for MCT aggregates with mass =  $11.6 \text{ ESD}^{0.22}$  ( $r^2=0.37$ ). No significant relationship between mass and size was determined for HCT aggregates.

## 3.2 Aggregate abundance and composition

### 3.2.1 Aggregate volume

The total amount of aggregate fraction that was isolated from the tanks, increased with increasing CO<sub>2</sub> concentration (Table 2). It was  $\sim 1.5$  times higher for the MCT and  $\sim 2.5$  times higher for the HCT compared to the LCT. This may partially be explained by increasing porosity and fragility of aggregates in MCT and HCT, leading to a higher amount of background suspension simultaneously harvested with the aggregates. To identify the total particulate volume attributed to aggregates solely (TPV), the cumulative volume of cells and particles within the aggregate fraction (AGG) was determined with the Coulter Multisizer. TPV was 2-fold higher in HCT than in MCT, and almost 4-fold higher than in LCT (Table 3), indicating that the amount of particles subjected to aggregation increased with increasing CO<sub>2</sub>.

### 3.2.2 Biogeochemistry of aggregates and bacterial abundance

Although TPV was highest in HCT, its total DW of  $38.2 \text{ mg L}^{-1}$  was almost the same as for the aggregate fractions of the other two treatments with  $39.9 \text{ mg L}^{-1}$  and  $37.4 \text{ mg L}^{-1}$  for LCT and MCT, respectively (Table 3). As a consequence, the ratio of DW to TPV was higher for aggregates in LCT (6.69), compared to MCT (3.09) and HCT (1.81). This can be explained by a higher contribution of PIC, since the density of CaCO<sub>3</sub> is  $\sim 2.7 \text{ g cm}^{-3}$  and hence higher than the average density of organic components (density of cytoplasm: 1.03–1.34 (Smayda, 1970)). Accordingly, the PIC/POC ratio of aggregates in HCT was only 0.023, and therewith about 5 times smaller than in LCT aggregates (PIC/POC=0.127). Again, PIC/POC for MCT aggregates was intermediate between LCT and HCT,

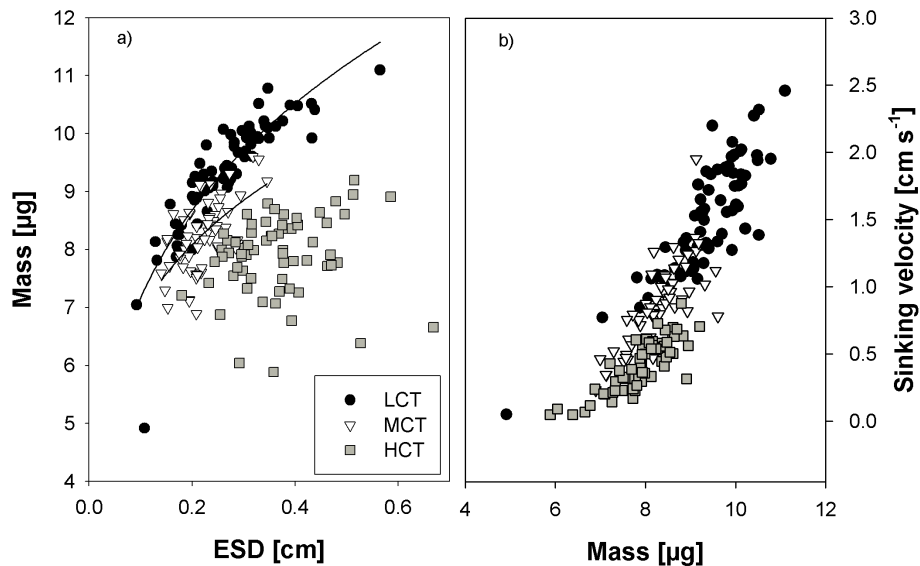


**Fig. 4.** Mass ( $\mu\text{g}$ ) of aggregates in relation to (a) their equivalent spherical diameter (ESD, cm) and (b) to their sinking velocity ( $\text{cm s}^{-1}$ ) in the three CO<sub>2</sub> treatments during the roller table experiments. (For  $n$  see Fig. 1). For LCT, mass of aggregates was related to the ESD with the power function  $y=13.6x^{0.28}$  ( $r^2=0.79$ ). The relationship of mass for the MCT aggregates was less pronounced with  $y=11.6x^{0.22}$  ( $r^2=0.37$ ).

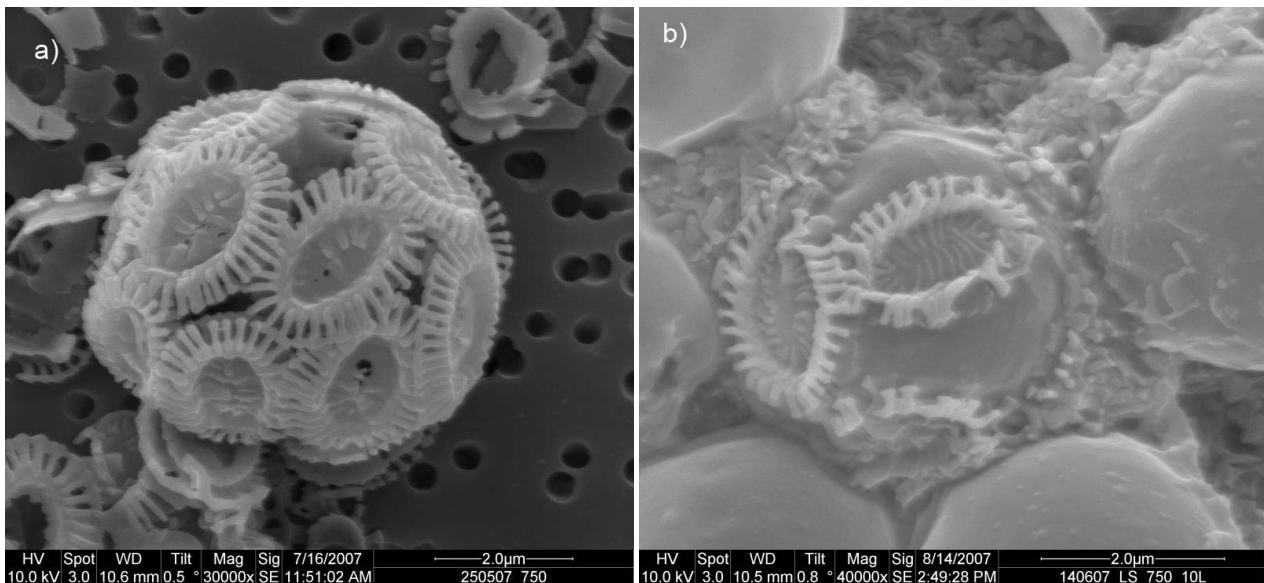


**Fig. 5.** SEM pictures of a calcified *E. huxleyi* from the beginning of the CO<sub>2</sub>-inoculation (T0) (left, a) and from the HCT of the suspension at the end of the aggregation experiment (T21) (right, b). This “missing link” indicates a defragmentation or detachment of coccoliths.

yielding a 3 times higher ratio than for HCT. By relating PIC to TPV, the density fraction of PIC within aggregates was calculated, yielding  $0.026 \text{ mg mm}^{-3}$  for LCT and 4 times lower values for HCT ( $0.007 \text{ mg mm}^{-3}$ ). PIC to TPV for MCT aggregates was  $\sim$  half as high compared to LCT ( $0.017 \text{ mg mm}^{-3}$ ). The density fraction of POC, however, was on average 1.5-fold higher for MCT and HCT, compared to LCT ( $0.209 \text{ mg mm}^{-3}$ ). The contribution of POC to TPC

was about 89 % for LCT aggregates, 96% for MCT, and almost 100% for HCT aggregates.

Overall, these ratios clearly demonstrated that the POC fraction in aggregates increased when going from LCT to HCT, while the PIC fraction decreased. Comparing the chemical composition of aggregates with the initial cell suspension (Table 1) showed that the POC content was already higher in MCT and HCT than in LCT before the onset of

**Table 3.** Results per litre tank volume of the chemical and biological analysis of the aggregate fraction (AGG) and enrichment factor (*f*) in aggregates after the roller tank experiment (T21).

Parameter	Unit	LCT	<i>f</i>	MCT	<i>f</i>	HCT	<i>f</i>
		AGG		AGG		AGG	
TPV	mm <sup>3</sup> L <sup>-1</sup>	5.77±0.921	10	10.2±3.55	8	19.5±6.33	12
TPC	mg L <sup>-1</sup>	1.37±0.353	11	3.19±0.804	13	5.83±1.45	12
POC	mg L <sup>-1</sup>	1.22±0.328	16	3.01±0.507	16	5.81±1.41	13
PIC	mg L <sup>-1</sup>	0.150±0.100	2.8	0.215±0.303	4.0	0.130±0.095	2.0
PN	mg L <sup>-1</sup>	0.134±0.048	16	0.147±0.035	13	0.311±0.095	11
DW	mg L <sup>-1</sup>	39.9±15.8	7.2	37.4±15.2	6.5	38.2±16.5	2.0
Bacteria	10 <sup>8</sup> L <sup>-1</sup>	2.77±1.22	56	3.45±1.76	38	5.51±3.03	28
DW/TPV	mg mm <sup>-3</sup>	6.69±3.83	0.66	3.09±0.104	0.85	1.81±0.334	0.16
PIC/TPV	mg mm <sup>-3</sup>	0.026±0.018	0.30	0.017±0.021	0.69	0.007±0.004	0.18
POC/TPV	mg mm <sup>-3</sup>	0.209±0.022	1.6	0.310±0.066	2.7	0.307±0.051	1.1
PIC/POC	mol/mol	0.127±0.096	0.19	0.063±0.084	0.53	0.023±0.017	0.17
POC/PN	mol/mol	11.8±1.84	0.98	25.9±2.11	1.2	24.0±4.01	1.2
POC/TPC	mol/mol	0.890±0.082	1.5	0.957±0.084	1.2	0.997±0.023	1.1
CO <sub>2</sub>	µmol L <sup>-1</sup>	1.24±0.968	–	18.4±4.74	–	53.1±8.46	–
Ω <sub>calcite</sub>	–	4.2±1.0	–	1.4±0.1	–	1.1±0.1	–

the roller table experiment. The PIC/POC ratio of the cell suspensions yielded on average 0.6 for LCT, 0.4 for MCT and 0.3 for HCT (Table 1), suggesting that the differences in aggregate composition were related to the different growth conditions for *E. huxleyi* rather than to differential aggregation of PIC and POC. The ratio of POC/PN was twice as high for cell suspension and aggregates in MCT and HCT compared to LCT (Tables 1, 3).

We also calculated enrichment factors (*f*) to describe the selective enrichment of a component in aggregates compared to the background suspension. The results show only small differences between the CO<sub>2</sub> treatments, except for the PIC density fraction, i.e. the ratio of PIC to TPV. Here, *f*<sub>PIC</sub> was lowest for HCT aggregates compared to MCT and LCT (Table 3), suggesting either a lower aggregation rate of PIC in this treatment or PIC dissolution within aggregates. Absolute abundance of bacteria was significantly higher in HCT than in LCT aggregates, yielding  $5.5 \times 10^8$  L ( $p < 0.05$  ANOVA & K.W.-Test) (Table 3).

At the end of the roller table experiment (T21), values for Ω<sub>calcite</sub> had dropped to 4.2 for LCT, 1.4 for MCT and 1.1 for HCT. This maybe attributed to bacterial respiration in the tanks. Significant dissolution of calcite during the incubation was unlikely, since Ω always stayed above 1, but cannot be excluded for microzones within the aggregates.

### 3.2.3 Scanning Electron Microscopy (SEM)

Figure 5a shows a typical *E. huxleyi* cell as observed in all treatments during the growth phase from T0 to T6. At the sampling date T14 “naked” cells, i.e. cells without coccoliths, appeared in all treatments (Fig. 5b). However,

in the LCT well formed coccoliths dominated, while non-calcifying cells were readily abundant in MCT and HCT. We also observed cells with residues of coccoliths (Fig. 5b).

## 4 Discussion

### 4.1 Effect of CO<sub>2</sub> on aggregate sinking velocity

Our study showed that exposure to different CO<sub>2</sub> concentrations during cell growth can affect properties and therefore sinking velocities of aggregates of *E. huxleyi*. Increasing CO<sub>2</sub> concentration reduced the PIC content and increased the POC content of cell suspension and aggregates as well. On average, sinking velocities were highest for LCT aggregates. MCT aggregates sank about half as fast as LCT aggregates. Lowest sinking velocities were observed for HCT aggregates, although these aggregates reached the greatest sizes in this experiment (Fig. 1). Interestingly, sinking velocity was clearly different between HCT and MCT, although differences in the degree of calcite ballast, as inferred from PIC/POC, were rather small.

Sinking velocity of aggregates in the ocean is highly variable, ranging from a few to several hundred meters per day, depending on e.g. the location, currents and composition (Fowler and Knauer, 1986; Ploug et al., 2008; Fischer and Karakaş, 2009). Engel et al. (2009b) determined sinking velocities of aggregates of calcified and of naked *E. huxleyi*, and observed rates of 1.0 to 2.5 cm s<sup>-1</sup> for ~0.1 cm aggregates derived from calcified cells, and a wider range, from 0.1 to 2.0 cm s<sup>-1</sup>, for aggregates from non-calcified cells of sizes ~0.1 to 1.0 cm. During this study, we determined a



similar range of sinking velocity and sizes for LCT and HCT aggregates that contained only marginal amounts of calcite. Compared to field-sampled marine snow settling velocities of HCT aggregates were within the range of natural aggregates (Ploug et al., 2008; Fischer and Karakaş, 2009).

Porosities of all aggregates of this experiment were, although in the upper range, comparable to porosities observed for field aggregates. Reports of marine snow porosities and of porosities derived from phytoplankton cultures range from >95 to 99.9% (Alldredge and Gotschalk, 1988; Engel and Schartau, 1999; Ploug et al., 2008). Average porosities of *E. huxleyi* aggregates were reported to be 95.9% and 99.6% for a calcifying and a non-calcifying strain, respectively (Engel et al., 2009b).

During this study, size of aggregates differed between treatments, although non-consistently. HCT aggregates reached the largest dimensions, being even larger than the LCT aggregates. A significant correlation between size ( $x$ , ESD, cm) and sinking velocity ( $y$ , cm s<sup>-1</sup>) was determined for aggregates of the LCT treatment only, yielding  $y=3.75x^{0.7}$  (Fig. 2). MCT aggregates showed a weak increase of settling velocity with size, while no change was observed for sinking rates of HCT aggregates over the whole size range (Fig. 2). For comparison, earlier studies yielded  $y=1.94x^{0.89}$  for a non-calcifying strain of *E. huxleyi* and  $y=3.5x^{0.33}$  for a calcifying strain (Engel et al., 2009b). The sinking velocity (m d<sup>-1</sup>) of natural marine snow that was investigated by Alldredge and Gotschalk (1988) increased with particle diameter (mm) according to  $y=50x^{0.26}$ .

Due to fractal scaling, the porosity of an aggregate increases with size in a non-linear function (Alldredge and Gotschalk, 1988). Hence, in order to evaluate the effect of CO<sub>2</sub> induced changes in chemical composition on aggregate properties, it is meaningful to compare aggregates of similar sizes. For mass of aggregates, this clearly revealed decreasing values when going from LCT over MCT to HCT (Fig. 4). Thereby, mass of MCT was more similar to HCT than to LCT, which agrees well with the chemical composition changes, e.g. the PIC density fraction. We also observed a higher variability in mass for HCT aggregates, than for MCT or LCT. From SEM pictures, we noticed that some cells in HCT had residues of coccoliths, while others were fully non-calcified. This could indicate that the amount of calcite in HCT aggregates was quite variable, leading to the observed higher variability in aggregate mass.

It has been suggested that the presence of lithogenic material could reduce the size and therewith the sinking velocity of aggregates, resulting in lower transport of aggregated material to depth (Passow and De La Rocha, 2006). Hamm (2002) observed that aggregate size decreased after addition of lithogenic particles, but that sinking velocity increased unless size was reduced by a factor of 20 at the highest mineral additions. Ploug et al. (2008) measured sinking velocities and other aggregate properties of marine snow, laboratory-made aggregates formed by diatoms or coccolithophores, and

zooplankton fecal pellets. They conclude that sinking velocities of aggregates depend on composition and density rather than on size. Here, we observed that mass of aggregates decreased when going from low to high CO<sub>2</sub> treatments, clearly resulting in lower sinking velocities at HCT (Fig. 4a, b). Higher mineral content of particles increased the mass of aggregates due to both, a reduction of porosity (Fig. 1) and a higher density of source particles (Table 3). As a consequence, mass of LCT aggregates with higher calcite content was higher than similar sized aggregates in MCT, and increased more strongly with size (Fig. 4a).

From a more general perspective, an increase in size does not necessarily have to result in higher sinking velocity for marine particle aggregates of high porosity. As porosity increases with size, the density of an aggregate decreases. An increase in size can only increase sinking velocity if  $d(r^2)/d(\Delta\rho) > 1$ , hence if the increase in size is larger than the decrease in excess density. Comparing MCT and HCT, we observed that  $\Delta\rho$  changed by a factor of about 4, while  $r^2$  changed roughly by a factor of 2. Hence, changes in size could not offset changes in the ballast effect during our study.

Comparing HCT and MCT, we noticed that the presence of even a little bit more PIC in MCT increased aggregate mass significantly. This suggests that the properties and the physical behaviour of an aggregate, i.e. its sinking velocity, are highly sensitive to even small changes in aggregate composition, such as expected for ocean acidification.

#### 4.2 Effect of CO<sub>2</sub> on the chemical composition of aggregates and the optical assessment of aggregates by SEM

Biogeochemical analyses showed that the ratio of particulate inorganic carbon (PIC) to particulate organic carbon (POC) was lowest for the HCT aggregate fraction compared to MCT and LCT. The decrease of PIC/POC ratios in *E. huxleyi* due to increased CO<sub>2</sub> conditions has been observed earlier and was attributed to more pronounced POC production combined with a decrease in calcification rate (Riebesell et al., 2000; Zondervan et al., 2001, 2002). However, other studies found no effect of CO<sub>2</sub> on PIC/POC ratios (Sciandra et al., 2003).

PIC/POC ratios in these earlier studies ranged from 0.77 to 1.02 at CO<sub>2</sub> concentrations of 27 to 6 µmol L<sup>-1</sup> and were thus much higher than ratios observed during our experiment (0.02 to 0.58 at 62 to 0.1 µmol L<sup>-1</sup> CO<sub>2</sub>). A large range of PIC/POC ratios was also determined for the cells of the coccolithophore *Gephyrocapsa oceanica*, ranging from 0.17 to 1.18 at CO<sub>2</sub> concentration between 33.7 to 5.7 µmol L<sup>-1</sup> (Zondervan et al., 2001). PIC/POC ratios for LCT at T21 were comparable to those observed during an *E. huxleyi* bloom that was followed in the course of an outdoor mesocosm experiment (i.e. 0.23–0.29; Engel et al., 2005). In the field, phytoplankton blooms often harbour a mixture of different taxa, including *E. huxleyi*. Here, PIC/POC

ratios smaller than 0.25 are not uncommon (Marañón and González, 1997).

The largest TPV was observed for aggregates in the HCT. Despite that, the DW of the HCT aggregate fraction was the lowest of the three CO<sub>2</sub> treatments. The elevated TPV in MCT and HCT was likely due to an enhanced POC production. The Redfield ratio for carbon to nitrogen of 6.6 was only observed for cell suspensions at the very beginning of the incubation (data not shown). The POC to PN ratio of the aggregate fraction at T21 was well above the Redfield ratio for the LCT, and even 3-fold higher for MCT and HCT. It has been suggested that C to N ratios increase in response to rising CO<sub>2</sub> concentration in a future ocean, mainly due to an enhanced organic carbon production (Hein and Sand-Jensen, 1997; Engel, 2002; Engel et al., 2005; Delille et al., 2005; Riebesell et al., 2007). During this experiment an increased production of POC coincided with a decrease in mineral ballast in form of CaCO<sub>3</sub>.

It has been proposed that vertical transport of aggregates is triggered by POC and not by lithogenic ballast (Berelson, 2002; Passow, 2004). Following these arguments, a higher amount of POC in the sea could favour the aggregation of other mineral particulates already present in the water column, which may especially be the case in coastal areas and those receiving a high rate of atmospheric deposition.

During this study, the large amount of aggregates in the HCT contained also the largest amount of associated bacteria. These results are consistent, since the HCT aggregates provided the largest area for bacterial attachment due to their large size and porosity, and also a higher amount of POC. It was shown earlier that degradation was enhanced in aggregates of non-calcified compared to calcified cells (Engel et al., 2009a). If a loss of calcite reduces the protection of organic matter from bacterial degradation, HCT aggregates may be subject to enhanced degradation. Hence, if representative for the future ocean, a CO<sub>2</sub> induced loss in aggregate calcite may also affect organic matter export due to its effect on the lability of organic components.

SEM pictures of the aggregates supported the findings of the biogeochemical analysis: whereas the SEM pictures of LCT aggregates readily showed coccoliths, very few coccoliths could be identified in HCT aggregates. Moreover, the SEM pictures of HCT aggregates showed a large number of naked cells. It has been reported earlier that changes in coccoliths morphology and reduced calcification of coccolithophores occur in response to high CO<sub>2</sub> treatments (Riebesell et al., 2000; Zondervan et al., 2001; Langer et al., 2006). Little is known, however, with respect to complete decalcification of coccolithophores under increased CO<sub>2</sub> concentrations. Though, there are reports of coccolithophores bearing only a few or one coccolith in dense natural blooms or senescent cultures (Paasche, 2002). It can't be excluded that the "naked" cells are haploid, non-calcifying S-cells, since the identification of S-cells and the distinction between both is difficult (Klaveness, 1972; Paasche, 2002). In a recent study

it was shown that viral infection induced lysis in calcified diploid *E. huxleyi* cells and the transition to the non-calcified haploid phase of *E. huxleyi* (Frada et al., 2008). If the loss of calcification in cells of our experiment would be due to viral infection, one can speculate that this may indicate that HCT cells are more susceptible to viral infection.

#### 4.3 Acclimation time scales and possible strain specific responses

In previous studies that investigated the physiology response of *E. huxleyi* to CO<sub>2</sub>, generation times ranged between 7 and 12 (Riebesell et al., 2000; Zondervan et al., 2001, 2002). A gradual increase in CO<sub>2</sub> concentration up to 1150 µatm for *E. huxleyi*, grown over 152 generations, however, did not change the cell's sensitivity to CO<sub>2</sub> or pH, and particular the changes in PIC/POC ratio (Müller et al., 2009). Compared to the shorter termed response, Barcelos e Ramos et al. (2009) report for *E. huxleyi* of a calcification decrease and organic carbon fixation increase with increasing CO<sub>2</sub> concentrations already within 8 to 14 h. The authors conclude that the (physiological) acclimation state is a matter of hours only. We therefore assume that the cells in this study were acclimated to the different CO<sub>2</sub>-conditions before transfer to the roller tanks.

So far, it is not known how fast natural populations of *E. huxleyi* can adapt to increasing *p*CO<sub>2</sub>. Therefore, we do not know whether adaption in situ will weaken or enhance the responses identified in short-termed experimental studies. Surely, more information is needed on the ability of coccolithophores to adapt to ocean acidification. However, including timescales of adaptation was beyond the scope of this experiment.

Langer et al. (2009) suggest that the difference in sensitivity of *E. huxleyi* to CO<sub>2</sub>-conditions is due to different genetic responses of strains of *E. huxleyi*. In this study the response of only one strain on different CO<sub>2</sub>-conditions was investigated. Nevertheless, if the response of another strain is opposite, e.g. increased PIC/POC, our study still provides information on how porosity and hence sinking velocity would be affected.

#### 4.4 Consequences for the carbon cycle and the efficiency of the biological pump

Based on our results, we infer that under high CO<sub>2</sub>-conditions, aggregate sinking velocity is reduced because of diminished ballast. Aggregates with lower sinking velocities prevail longer in the upper water column and are therefore more prone to grazing and decomposition. Applied to the future ocean, a possible scenario could thus be that the efficiency of POC export to deep waters associated to coccolithophore aggregates decreases. Since the total amount of organic carbon included in aggregates was higher under high CO<sub>2</sub>-conditions, more POC may be transported to

mid-depths, where it will be degraded by heterotrophic organisms. A higher consumption of oxygen at mid-depths due to the higher heterotrophic degradation activity could be one consequence. This future scenario thus points to a weakening of the biological pump at times of coccolithophore blooms, and to an increase of oxygen utilisation at mid-depths, provided that no other ballasting material, e.g. dust, would be available to balance the loss of biogenic calcite ballast.

## 5 Conclusion

Ocean acidification may induce changes in the quality of biogenic particles that in turn affect the formation and composition of aggregates and in consequence their properties and sinking velocity.

Our study on aggregate formation and sinking therewith provides an example how environmental changes, such as ocean acidification, can induce cascading effects in marine environments. Secondary effects of ocean acidification, such as changes in aggregate sinking speed, are complex and difficult to predict. The sensitivity of aggregate porosity to small changes in calcite ballast indicates that an environmental perturbation, here the CO<sub>2</sub> increase, may be amplified in subsequent processes.

Because aggregates efficiently export organic matter and organisms from the ocean's surface, future changes in aggregation dynamics and in aggregate export rate are going to transmit the signal of anthropogenic perturbation into the ocean's interior. However, this study was conducted with a single species, and conclusions on complex marine ecosystems have to be drawn with caution. As the biological diversity of natural systems is large, adaptations of organisms to environmental perturbations will occur and the signal of perturbation may diminish over time. Hence, for a better understanding of future ocean responses, more information is needed on secondary effects of global change, as well as on the progression of the perturbation over time and space.

*Acknowledgements.* This study was supported by the Helmholtz Association (contract no. HZ-NG-102) and by the Belgian Federal Science Policy Office in the framework of the PEACE project (contract no. SD/CS/03A/B). Thanks go to Mirko Lunau for his support with the flow cytometer measurements, to Nicole Händel for nutrient measurements, and to Steffi Koch for helping setting up the CO<sub>2</sub> aeration system. We also thank three anonymous reviewers for their helpful comments.

Edited by: J. Middelburg

## References

- Allredge, A. and Gotschalk, C.: In situ settling behaviour of marine snow, *Limnol. Oceanogr.*, 33(3), 339–351, 1988.
- Armstrong, R. A., Lee, C., Hedges, J. I., Honjo, S., and Wakeham, S. G.: A new, mechanistic model for organic carbon flux in the ocean based on the quantitative association of POC with ballast minerals, *Deep-Sea Res. Pt. II*, 49, 219–236, 2002.
- Barcelos e Ramos, J., Müller, M. N., and Riebesell, U.: Short-term response of the coccolithophore *Emiliania huxleyi* to an abrupt change in seawater carbon dioxide concentrations, *Biogeosciences*, 7, 177–186, 2010, <http://www.biogeosciences.net/7/177/2010/>.
- Berelson, W. A.: Particle settling rates increase with depth in the ocean, *Deep-Sea Res. Pt. II*, 49, 237–251, 2001.
- Brewer, P. G., Bradshaw, A. L., and Williams, R. T.: Measurements of total carbon dioxide and alkalinity in the North Atlantic in 1981, in: *The changing carbon cycle*, edited by: Trabalka, J. R. and Reichle, D. E., Springer, New York, 349–370, 1986.
- Delille, B., Harlay, J., Zondervan, I., Jacquet, S., Chou, L., Wollast, R., Bellerby, R. G. J., Frankignoulle, M., Borges, A. V., Riebesell, U., and Gattuso, J.-P.: Response of primary production and calcification to changes of pCO<sub>2</sub> during experimental blooms of the coccolithophorid *Emiliania huxleyi*, *Global Biogeochem. Cycles*, 19, GB2023, doi:10.1029/2004GB002318, 2005.
- Dietrich, G., Kalle, K., Krauss, W., and Siedler, G.: *Allgemeine Meereskunde: Eine Einführung in die Ozeanographie*, Gebrüder Borntraeger, Berlin, Stuttgart, 593 pp., 1975.
- Engel, A. and Schartau, M.: Influence of transparent exopolymer particles (TEP) on sinking velocity of *Nitzschia closterium* aggregates, *Mar. Ecol. Prog. Ser.*, 182, 69–76, 1999.
- Engel, A., Goldthwait, S., Passow, U., and Alldredge, A.: Temporal decoupling of carbon and nitrogen dynamics in a mesocosm diatom bloom, *Limnol. Oceanogr.*, 47(3), 753–761, 2002.
- Engel, A., Zondervan, I., Aerts, K., Beaufort, L., Benthien, A., Chou, L., Delille, B., Gattuso, J.-P., Harley, J., Heemann, C., Hoffmann, L., Jacquet, S., Nejstgaard, J., Pizay, M.-D., Rochelle-Newall, E., Schneider, U., Terbrüggen, A., and Riebesell, U.: Testing the direct effect of CO<sub>2</sub> concentration on a bloom of the coccolithophorid *Emiliania huxleyi* in mesocosm experiments, *Limnol. Oceanogr.*, 50(2), 493–507, 2005.
- Engel, A., Abramson, L., Szlosek, J., Liu, Z., Stewart, G., Hirschberg, D., and Lee, C.: Investigating the effect of ballasting by CaCO<sub>3</sub> in *Emiliania huxleyi*, II: Decomposition of particulate organic matter, *Deep-Sea Res. Pt. II*, 56(18), 1408–1419, doi:10.1016/j.dsr2.2008.028, 2009a.
- Engel, A., Szlosek, J., Abramson, L., Liu, Z., and Lee, C.: Investigating the effect of ballasting by CaCO<sub>3</sub> in *Emiliania huxleyi*: I. Formation, settling velocities and physical properties of aggregates, *Deep-Sea Res. Pt. II*, 56(18), 1397–1407, doi:10.1016/j.dsr2.2008.027, 2009b.
- Fischer, G. and Karakaş, G.: Sinking rates and ballast composition of particles in the Atlantic Ocean: implications for the organic carbon fluxes to the deep ocean, *Biogeosciences*, 6, 85–102, 2009, <http://www.biogeosciences.net/6/85/2009/>.
- Fowler, S. W. and Knauer, G. A.: Role of large particles in the transport of elements and organic compounds through the oceanic water column, *Prog. Oceanogr.*, 16, 147–194, 1986.
- Frada, M., Probert, I., Allen, M. J., Wilson, W. H., and de Vargas, C.: The “Cheshire Cat” escape strategy of the coccolithophore *Emiliania huxleyi* in response to viral infection, *PNAS*, 105(41), 15944–15949, 2008.
- Francois, R., Honjo, S., Krishfield, R., and Manganini, S.: Factors controlling the flux of organic carbon to the bathypelagic

- zone of the ocean, *Global Biogeochem. Cycles*, 16(4), 1087, doi:10.1029/2001GB001722, 2002.
- Gasol, J. M. and del Giorgio, P. A.: Using flow cytometry for counting natural planktonic bacteria and understanding the structure of planktonic bacterial communities, *Sci. Mar.*, 64(2), 197–224, 2000.
- Gran, G.: Determination of the equivalence point in potentiometric titrations, part II, *Analyst*, 77, 661–671, 1952.
- Grasshoff, K., Kremling, K., and Ehrhardt, M., with contributions by Anderson, L. G.: *Methods of seawater analysis*, third edn., Wiley-VCH, Weinheim, 1999.
- Guillard, R. R. and Rytner, J. H.: Studies of marine planktonic diatoms, I. *Cyclotella nana* Hustedt and *Detonula confervacea* (Cleve) Gran, *Can. J. Mikrobiol.*, 8, 229–239, 1962.
- Hamm, C. E.: Interactive aggregation and sedimentation of diatoms and clay-sized lithogenic material, *Limnol. Oceanogr.*, 47(6), 1790–1795, 2002.
- Hein, M. and Sand-Jensen, K.: CO<sub>2</sub> increases oceanic primary production, *Nature*, 388, 526–527, 1997.
- Holligan, P. M., Viollier, M., Harbour, D. S., Camus, P., and Champagne-Philippe, M.: Satellite and ship studies of coccolithophore production along a continental shelf edge, *Nature*, 304, 339–342, 1983.
- Honjo, S., Manganini, S. J., and Cole, J. J.: Sedimentation of biogenic matter in the deep ocean, *Deep-Sea Res.*, 29(5), 609–625, 1982.
- Iglesias-Rodriguez, M. D., Halloran, P. R., Rickaby, R. E. M., Hall, I. R., Colmenero-Hidalgo, E., Gittins, J. R., Green, D. R. H., Tyrell, T., Gibbs, S. J., von Dassow, P., Rehm, E., Armbrust, E. V., and Boessenkool, K. P.: Phytoplankton in a High-CO<sub>2</sub> World, *Science*, 320, 336–340, 2008.
- IPCC: *Climate Change 2001: The Scientific Basis. Contribution of working group I to the third assessment report of the Intergovernmental Panel on Climate Change*, edited by: Houghton, J. T., Ding, Y., Griggs, D. J., Noguer, M., van der Linden, P. J., Dai, X., Maskell, K., and Johnson, C. A., Cambridge University Press, Cambridge, United Kingdom and New York, NY, USA, 881 pp, 2001.
- Ittekkot, V. and Haake, B.: The terrestrial link in the removal of organic carbon in the sea. In: *Facets of Modern Biogeochemistry*, edited by: Ittekkot, V., Kempe, S., Michaelis, M., and Spitz, A., Springer, Berlin, 318–325, 1990.
- Klaas, C. and Archer, D. E.: Association of sinking organic matter with various types of mineral ballast in the deep sea: Implications for the rain ratio, *Global Biogeochem. Cycles*, 16(4), 1116, doi:10.1029/2001GB001765, 2002.
- Klavens, D.: *Coccolithus huxleyi* (Lohm.) Kamptn, II. The flagellate cell, aberrant cell types, vegetative propagation and life cycles, *Br. Phycol. J.*, 7, 309–318, 1972.
- Kleypas, J. A., Feely, R. A., Fabry, V. J., Langdon, C., Sabine, C. L., and Robbins, L. L.: Impacts of ocean acidification on coral reefs and other marine calcifiers: A guide for future research, report of a workshop held 18–20 April 2005, St. Petersburg, FL, sponsored by NSF, NOAA and the US Geological Survey, 88 pp., 2006.
- Langer, G., Geisen, M., Baumann, K.-H., Kläs, J., Riebesell, U., Thoms, S., and Young, J. R.: Species-specific responses of calcifying algae to changing seawater carbonate chemistry, *Geochem. Geophys. Geosy.*, 7(9), Q04002, doi:10.1029/2005GC001227, 2006.
- Langer, G., Nehrke, G., Probert, I., Ly, J., and Ziveri, P.: Strain-specific responses of *Emiliana huxleyi* to changing seawater carbonate chemistry, *Biogeosciences*, 6, 2637–2646, 2009, <http://www.biogeosciences.net/6/2637/2009/>.
- Lewis, E. and Wallace, D. W. R.: Program developed for CO<sub>2</sub> system calculations. ORNL/CDIAC-105, Carbon dioxide information analysis centre, Oak Ridge National Laboratory, US Department of Energy, Oak Ridge, Tennessee, 1998.
- Marañón, E. and González, N.: Primary production, calcification and macromolecular synthesis in a bloom of the coccolithophore *Emiliana huxleyi* in the North Sea, *Mar. Ecol. Prog. Ser.*, 157, 61–77, 1997.
- Müller, M. N., Schulz, K. G., and Riebesell, U.: Effects of long-term high CO<sub>2</sub> exposure on two species of coccolithophores, *Biogeosciences Discuss.*, 6, 10963–10982, 2009, <http://www.biogeosciences-discuss.net/6/10963/2009/>.
- Paasche, E.: A review of the coccolithophorid *Emiliana huxleyi* (Prymnesiophyceae), with particular reference to growth, coccolith formation, and calcification-photosynthesis interactions, *Phycologia*, 40(6), 503–529, 2002.
- Passow, U.: Switching perspectives: Do mineral fluxes determine particulate organic carbon fluxes or vice versa? *Geochem. Geophys. Geosy.*, 5(4), Q04002, doi:10.1029/2003GC000670, 2004.
- Passow, U. and De La Rocha, C. L.: Accumulation of mineral ballast on organic aggregates, *Global Biogeochem. Cycles*, 20, GB1013, doi:10.1029/2005GB002579, 2006.
- Ploug, H. and Iversen, M. H.: Ballast, sinking velocity, and apparent diffusivity within marine snow and zooplankton fecal pellets: Implications for substrate turnover by attached bacteria, *Limnol. Oceanogr.*, 53(5), 1878–1886, 2008.
- Raitos, D. E., Lavender, S. J., Pradhan, Y., Tyrell, T., Reid, P. C., and Edwards, M.: Coccolithophore bloom size variation in response to the regional environment of the subarctic North Atlantic, *Limnol. Oceanogr.*, 51(5), 2122–2130, 2006.
- Redfield, A. C., Ketchum, B. M., and Richards, F. A.: The influence of organism on the composition of sea-water. In: *The Sea*, edited by: Hill, M. N., John Wiley & Sons, New York, 26–77, 1963.
- Riebesell, U., Zondervan, I., Rost, B., Tortell, P. D., Zeebe, R. E., and Morel, F. M. M.: Reduced calcification of marine plankton in response to increased atmospheric CO<sub>2</sub>, *Nature*, 407, 364–367, 2000.
- Riebesell, U., Schulz, K. G., Bellerby, R. G. J., Botros, M., Fritsche, P., Meyerhöfer, M., Neill, C., Nondal, G., Oschlies, A., Wohlers, J., and Zöllner, E.: Enhanced biological carbon consumption in a high CO<sub>2</sub> ocean, *Nature*, 450, 545–548, 2007.
- Robertson, J. E., Robinson, C., Turner, D. R., Holligan, P., Watson, A. J., Boyd, P., Fernandez, E., and Finch, M.: The impact of a coccolithophore bloom on oceanic carbon uptake in the northeast Atlantic during summer 1991, *Deep-Sea Res. Pt. I.*, 41(2), 297–314, 1994.
- Rost, B., Riebesell, U., and Burkhardt, S.: Carbon acquisition of bloom-forming marine phytoplankton, *Limnol. Oceanogr.*, 48(1), 55–67, 2003.
- Sabine, C. L., Feely, R. A., Gruber, N., Key, R. M., Lee, K., Bullister, J. L., Wanninkhof, R., Wong, C. S., Wallace, D. W. R., Tilbrook, B., Millero, F. J., Peng, T.-H., Kozyr, A., Ono, T., and Rios, A. F.: The oceanic sink for anthropogenic CO<sub>2</sub>, *Science*, 305, 367–371, 2004.

- Sciandra, A., Harlay, J., Lefèvre, D., Lemée, R., Rimmelin, P., Denis, M., and Gattuso, J.-P.: Response of coccolithophorid *Emiliana huxleyi* to elevated partial pressure of CO<sub>2</sub> under nitrogen limitation, *Mar. Ecol.-Prog. Ser.*, 261, 111–122, 2003.
- Smayda, T. J.: The suspension and sinking of phytoplankton in the sea, *Oceanogr. Mar. Biol. Ann. Rev.*, 8, 353–414, 1970.
- Tooby, P. F., Wick, G. L., and Isaacs, J. D.: The Motion of a small sphere in a rotating velocity field: a possible mechanism for suspending particles in turbulence, *J. Geophys. Res.*, 82(15), 2096–2100, 1977.
- Van der Wal, P., Kempers, R. S., and Veldhuis, M. J. W.: Production and downward flux of organic matter and calcite in a North Sea bloom of the coccolithophore *Emiliana huxleyi*, *Mar. Ecol. Prog.-Ser.*, 126, 247–265, 1995.
- Winter, A., Jordan, R. W., and Roth, P. H.: Biogeography of living coccolithophores in ocean waters, in: *Coccolithophores*, edited by: Winter, A. and Siesser, W. G., Cambridge University Press, Cambridge, UK.
- Zondervan, I., Zeebe, R. E., Rost, B., and Riebesell, U.: Decreasing marine biogenic calcification: A negative feedback on rising atmospheric pCO<sub>2</sub>, *Global Biogeochem. Cycles*, 15(2), 507–516, 2001.
- Zondervan, I., Rost, B., and Riebesell, U.: Effect of CO<sub>2</sub> concentration on the PIC/POC ratio in the coccolithophore *Emiliana huxleyi* grown under light-limiting conditions and different day lengths, *J. Exp. Mar. Biol. Ecol.*, 272, 55–70, 2002.